Journal of
Synchrotron
Radiation

ISSN 0909-0495

Received 6 July 2009
Accepted 23 November 2009

Diffractive–refractive optics: low-aberration Bragg-case focusing by precise parabolic surfaces

P. Oberta,[a,b]* P. Mikulík,[c] M. Kittler,[a] J. Hrdý[a] and L. Peverini[d]

[a]Institute of Physics, Academy of Sciences of the Czech Republic v.v.i., CZ-18221 Praha 8, Czech Republic, [b]Swiss Light Source, Paul Scherrer Institut, CH-5232 Villigen, Switzerland, [c]Department of Condensed Matter Physics, Faculty of Sciences, Masaryk University, CZ-61137 Brno, Czech Republic, and [d]ESRF, FR-38043 Grenoble, France. E-mail: peter.oberta@psi.ch

Based on analytical formulae calculations and ray-tracing simulations a low-aberration focal spot with a high demagnification ratio was predicted for a diffractive–refractive crystal optics device with parabolic surfaces. Two Si(111) crystals with two precise parabolic-shaped grooves have been prepared and arranged in a dispersive position (+,−,−,+) with high asymmetry. Experimental testing of the device at beamline BM05 at the ESRF provided a focal spot size of 38.25 µm at a focal distance of 1.4 m for 7.31 keV. This is the first experiment with a parabolic-shaped groove; all previous experiments were performed with circular grooves which introduced extreme aberration broadening of the focal spot. The calculated and simulated focal size was 10.8 µm at a distance of 1.1 m at 7.31 keV. It is assumed that the difference between the measured and calculated/simulated focal spot size and focal distance is due to insufficient surface quality and to alignment imperfection.

Keywords: diffractive–refractive optics; aberration; parabolic groove.

1. Introduction

One of the main functions of synchrotron optics is to modulate the beam shape and direction. A very important feature of an optical system is the potential of sagittal focusing. One possibility is to use a bent crystal, as was developed by Sparks *et al.* (1982). In this case, sagittal focusing is realised by dynamical bending of the second crystal. Another possibility is to use diffractive–refractive optics. Here, sagittal focusing occurs due to diffraction on a shaped surface, where the surface shape is realised by drilling tools and not by bending. On the crystal walls, which are tilted with respect to the crystallographic planes, non-coplanar diffraction and, at the same time, refraction occurs which slightly changes the direction of the diffracted beam. This change of exit beam path can be used for sagittal focusing, as was demonstrated by Hrdý & Siddons (1999) and Hrdý (1998). Focusing based on diffractive–refractive optics was also studied and experimentally proved in the Laue regime (Hrdý *et al.*, 2006). It was found that sagittal focusing occurs with the correct crystal surface shape: a longitudinal parabolic groove.

A problem of refraction is the sagittal spread of the diffracted beam, which broadens the diffracted beam and makes the focus unsharp. To avoid this broadening of the focus a dispersive arrangement of the crystals (Beaumont & Hart, 1974) (+,−,−,+) is desired. Also Hrdý & Siddons (1999) showed that the sagittal broadening introduced by the diffractive–refractive effect can be cancelled using a dispersive arrangement of the crystals (Fig. 1). According to the dynamical theory, a crystal accepts the wavelength λ in a certain angular region delimited by the beams 1 (lower θ) and 2 (higher θ). In the case of some inclination β the diffracted beams are sagittally deviated from the plane of diffraction. The beam at the middle of the region is deviated by δ, beam 1 is sagittally deviated by the angle $\delta - \Delta$ and beam 2 is

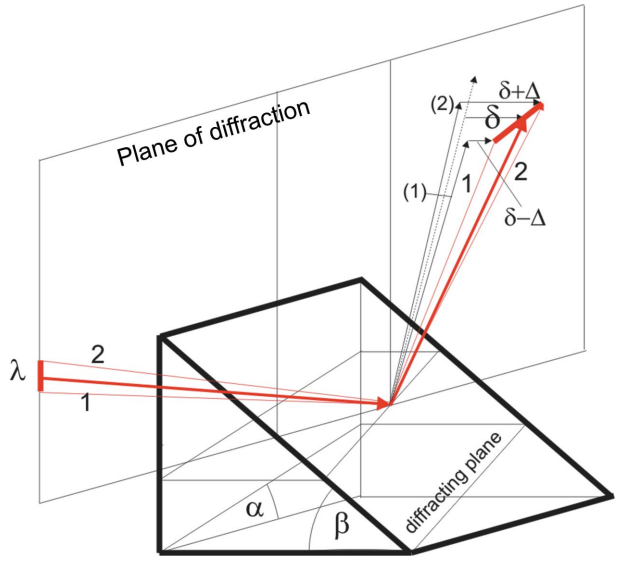

Figure 1
Geometrical construction of the sagittal spread cancellation.

deviated by the angle $\delta + \Delta$. The total sagittal spread is 2Δ. (For the symmetrical case, *i.e.* $\beta = 0$, the diffracted region is delimited by beams 1 and 2.) If we put the second crystal at the dispersive position, the beam at the middle of the region is deviated again by δ, so that the total deviation is 2δ. However, beam 1, impinging on the first crystal on the low-θ side of the diffraction region, impinges on the second crystal on the high-θ side of the diffraction region and thus it is sagittally deviated by the angle $\delta + \Delta$ on the second crystal. This means that the total sagittal deviation is $\delta - \Delta + \delta + \Delta = 2\delta$. Similarly it may be shown that the sagittal deviation of beam 2 after diffraction from both crystals is also 2δ. This means that the dispersive setting of crystals cancels the sagittal spread introduced by one crystal.

If the shape of the crystal surface differs from a parabolic shape,

$$y = ax^2, \tag{1}$$

and the surface quality is insufficient; the aberrations are introduced. For asymmetric Bragg diffraction the focusing distance of the parabolic crystal system is

$$f = S/(2aNK'S - 1), \tag{2}$$

where S is the source-to-crystal distance, $N = 4$ is the number of diffraction events, a is a parameter from the parabola equation and

$$K' = K(2 + b + 1/b)/4\cos\alpha, \tag{3}$$

where

$$K = (2r_eF_0/\pi V)d_{hkl}\lambda = -\chi_0/\sin\Theta_B.$$

Here r_e is the classical electron radius, F_0 is the structure factor, χ_0 is the susceptibility, V is the unit-cell volume, λ is the wavelength, d_{hkl} is the distance of the atomic planes, α is the asymmetry angle ($\alpha > 0$ for the grazing-incidence case) and

$$b = \sin(\Theta - \alpha)/\sin(\Theta + \alpha). \tag{4}$$

When the arrangement of the crystals is as shown in Fig. 2, then the focusing equation (2) has to be corrected (Hrdý *et al.*, 2005) to

$$f_n = (-f_{n-1} + d_{n-1})/\left[2K'a_n(-f_{n-1} + d_{n-1}) - 1\right], \tag{5}$$

where f_n is the focusing distance after the nth crystal, f_{n-1} is the focusing distance of the $(n-1)$th crystal, d_{n-1} is the distance of the two crystals and a_n is the parabola parameter. (As can be seen from the equation, different parabolic shapes represented by different parameters a can also be included in the calculations.) This was simulated and confirmed by ray-tracing (Hrdý *et al.*, 2005).

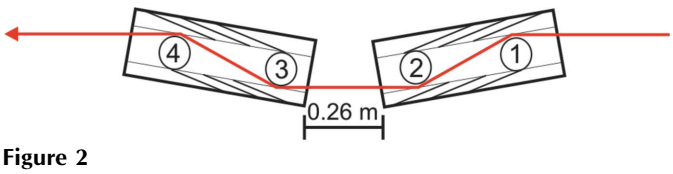

Figure 2
The double-crystal arrangement used, with four diffraction events.

Until recently, the available technology of drilling did not allow us to prepare the crystals with a precise parabolic surface shape. Therefore we prepared devices where the ideal parabolic shape was approximated by a circular shape. Such a device was tested by Artemiev *et al.* (2003) and the beam profile was demagnified 22 times to a diameter of 0.4 mm. The calculated beam diameter, *i.e.* the focal spot size, was 0.12 mm. The measured mismatch was 0.28 mm. In a different experiment (Hrdý *et al.*, 2001) the measured focus spot size was 0.418 mm whereas the calculated source size was 0.308 mm. The measured mismatch in both cases was due to aberration caused by the circular shape of the crystal surface instead of the ideal parabolic shape. Recent progress in drilling technology allowed us to prepare crystals with precise parabolic surface shapes (Hrdý & Oberta, 2008). The aim of this paper is to describe the focusing properties of a double-crystal device with four precise parabolic-shaped surfaces. Experimentally measured values of focus distance and focal spot size will be compared with analytical calculations and ray-tracing simulations.

2. Description of device and experimental arrangement

In this paper we describe our experiment where we used two crystals with a parabolic groove (Fig. 2) to experimentally verify the theoretical demagnification without aberration introduced by non-perfect crystal shape. The fabrication process is described in detail by Hrdý & Oberta (2008). The idea was to calculate and manufacture a precise parabolic profile of the groove. The crystals which we used were originally designed for focusing of 4 keV radiation, but the experiment could not be realised. However, it appeared that with a certain limitation of acceptance these crystals could be used for focusing 7 keV radiation at beamline BM05 at the ESRF.

It is very difficult to eliminate aberration completely in a focusing system, because there are multiple factors which create aberrations. The arrangement which was used (Fig. 1) introduces, in principle, low aberration because the beam is slightly sagittally deviated at each diffracting surface. Owing to these deviations the diffracted beam hits every parabola at a different point and the exit beam is only slightly displaced. This displacement is of the order of 10^{-4}, thus the exit beam displacement is of the order of micrometres. This geometrical aberration is very small. Another factor introducing aberration is the surface quality of the crystals.

We used two Si(111) crystals in an asymmetric arrangement, with an asymmetry angle of $\alpha = 15^\circ$; with a beam energy of 7.31 keV, then $\Theta_B = 15.7^\circ$. The impinging radiation formed an incident angle of 0.7° with the surface which meant that this arrangement is surface-sensitive (Hrdá *et al.*, 2003, 2005). The cut-off edge (creating an L-shape crystal) of the crystal (Fig. 3) was made because the acceptance angle at 7.31 keV is different compared with the acceptance angle at 4 keV for which the crystals dimensions were designed. Without this cut-off, the leaving diffracted radiation at 7.31 keV would hit the inner walls of the crystal. The advantage of this crystal is its

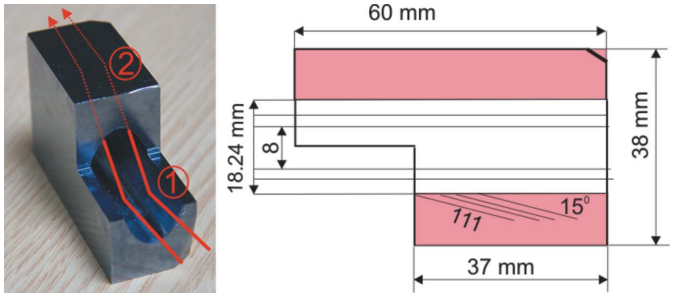

Figure 3
The parabolic-shaped crystal groove with cut-off edge.

large acceptance, which depends on the Bragg angle. For example, the acceptance for 5.28 keV is 9 mm. The crystal dimensions are 60 mm × 38 mm (L × H). The slit opening at the experiment was 5 mm × 1 mm (H × V).

3. Numerical simulations

We have performed ray-tracing simulations using the program *SKL*. This program is based on the dynamical theory of diffraction and the Monte Carlo approach. It was developed at Masaryk University and applied previously by Korytár *et al.* (2003) and others. Four different simulations have been made using a combination of point and real source size and monochromatic and polychromatic radiation. The real source had dimensions of 270 µm × 80 µm, which corresponds to beamline BM05 at the ESRF. The term 'polychromatic radiation' refers to a situation without a pre-monochromator. The difference in the results was in a slightly longer focal distance (a few mm) and the dimensions of the focal spot. Fig. 4 shows simulations of the point source with (*a*) monochromatic radiation and (*b*) polychromatic radiation. The colour scale indicates the intensity; the *x*- and *y*-axes are the spot dimensions in mm (camera perpendicular to beam). The monochromatic focus (Fig. 4*a*) is at a distance of 1.083 ± 0.005 m from the second crystal (5 mm is the simulated discrepancy) and the polychromatic focus (Fig. 4*b*) is at a distance of 1.088 ± 0.005 m.

The difference in the focal length for the monochromatic and polychromatic radiation is negligible; on the other hand the polychromatic spot is much broader than the monochromatic spot. This is to be expected because of different wavelengths diffracting under different angles. Because of the smaller focal size, a higher intensity is concentrated in the focal spot which makes the monochromatic focal spot 50 times brighter. Fig. 5 shows two finite source size (270 µm × 80 µm)

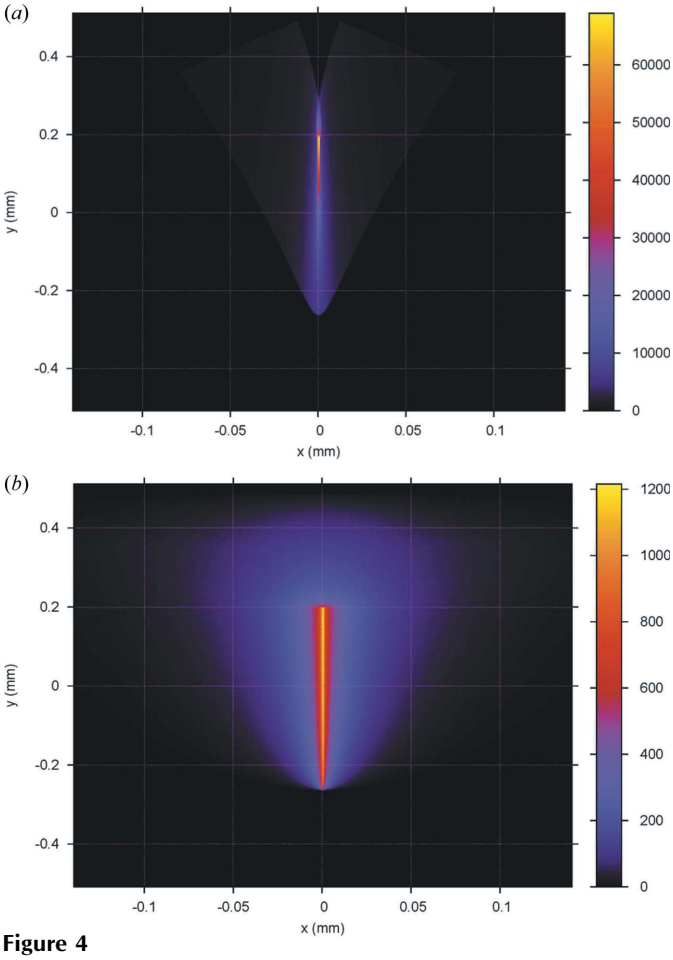

Figure 4
Ray-tracing simulations of a point source for the monochromatic case (*a*) and the polychromatic case (*b*).

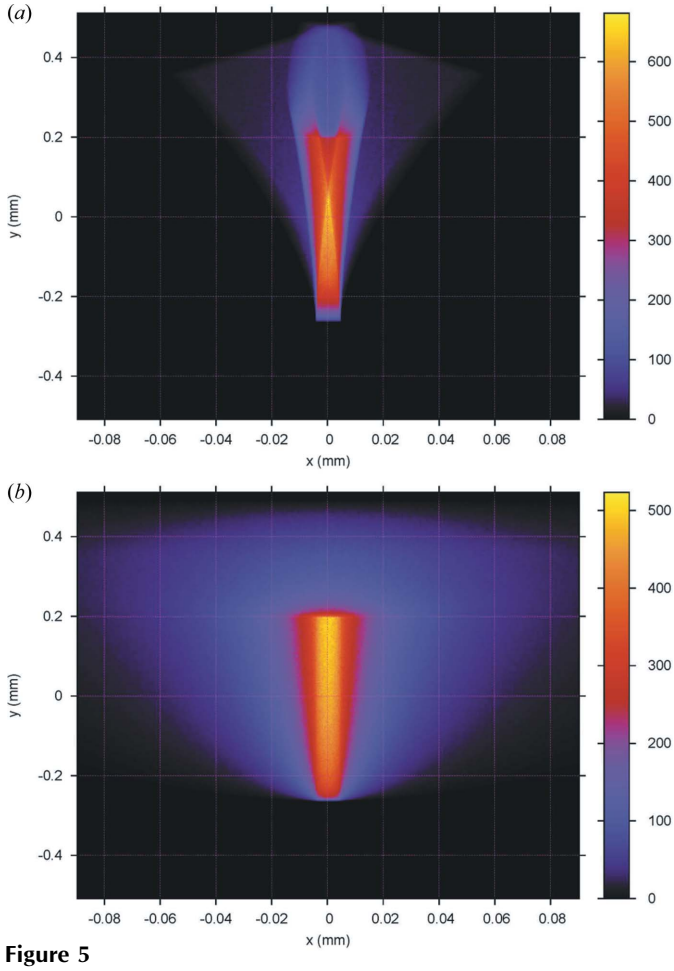

Figure 5
The ray-tracing simulations of a finite source for the monochromatic case (*a*) and the polychromatic case (*b*).

simulations, for the monochromatic source (*a*) and for the polychromatic source (*b*).

The focusing distance is 1.097 ± 0.005 m for the monochromatic radiation and 1.092 ± 0.005 m for the polychromatic radiation. The focal spot sizes, intensities and shapes are very similar.

4. Experiment

The experiment was performed at the ESRF at beamline BM05. This bending-magnet beamline has a source size of 270 µm × 80 µm. Fig. 6 shows a photograph of the arrangement of the crystals corresponding to the beam direction shown in Fig. 1. The front side of the second crystal was 34.901 m from the source. The shortest distance of faces of these two crystals was 0.26 m.

Both Bragg crystals had an asymmetry of 15° and, using an energy of 7.31 keV (Bragg angle 15.7°), we turned the crystals from the horizontal position (given by the primary beam) by only 0.7°. This grazing-incident arrangement (angle of incidence 0.7°) made the focal spot properties (shape and distance) very sensitive to surface imperfections and misalignments of the crystals.

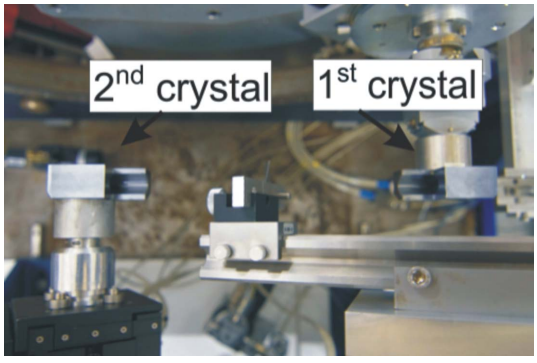

Figure 6
Picture of the crystal setting.

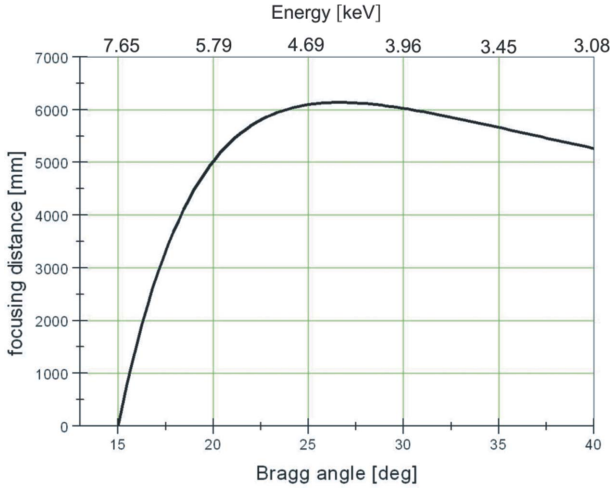

Figure 7
Dependence of focusing distance on the energy [scaled *via* the Si(111) Bragg angle].

Fig. 7 shows the dependence of the focusing distance f on energy according to equation (2), and also on the Bragg angle for Si(111). As can be seen from the figure, the crystal can be used over an energy range of approximately 3 –7.65 keV. For a fixed angle of asymmetry, one can change the focusing distance by changing the energy. The most important parameter in equation (2) is the source-to-crystal distance. The shorter this distance, the longer the focusing distance. The energy range can be tuned by changing the angle of asymmetry, but at the same time the focusing distance is growing. At a certain energy it grows to infinity; therefore the ideal working range is between 4 and 8 keV. The usable energy range is much smaller than that of, for example, a dynamically bent sagittally focusing optical system, but it is much simpler to operate (Sparks *et al.*, 1982; Krisch *et al.*, 1990). By using equation (2) the calculated focusing distance for 7.31 keV is 1.10 m. The experimentally measured focusing distance was 1.40 m, which is a mismatch of 0.3 m. This mismatch is caused by a non-precise alignment. Also some positioning mistakes are introduced by the fixing of the two crystals to the crystal holders with wax. The focusing distance of 1.4 m corresponds to a Bragg angle of 15.875°, which is a mismatch of 0.165° with the calculated angle of 15.7°. As one can see from the detail in Fig. 7, in the range of 15–25° the dependence of the focusing distance on the Bragg angle is very steep and even small changes in angle are responsible for a high change in the focusing distance. A change of angle by 0.165° can lead to a prolongation of the focusing distance by the measured 0.3 m. Fig. 8(*a*) shows the smallest focal spot we have detected. For comparison, Fig. 8(*b*) shows the focal spot in false colours (gradient map) to make the structure more visible, and Fig. 8(*c*) shows the simulated focal spot. As one can see, the simulation is very similar to the real picture.

As a detector we used a CCD camera with the following specifications: PCO2000, CCD chip KAI4020, 2048 × 2048 pixels, 14-bit ADC. The nominal pixel size given by the manufacturer was 7.4 µm, whereas we measured a pixel size of 8.5 µm; we will use the measured value. The image in Fig. 8(*a*) was taken with an exposure time of 30 s. The intensity profile of the spot showed a peak of almost 900 counts (30 counts s^{-1}) in the centre of the focal spot. The diameter of the focal spot was 4.5 pixels. When we took into account our pixel size, then the spot had a diameter of 38.25 µm (33.3 µm nominal pixel value). The crystal-to-source distance was 34.901 m and the

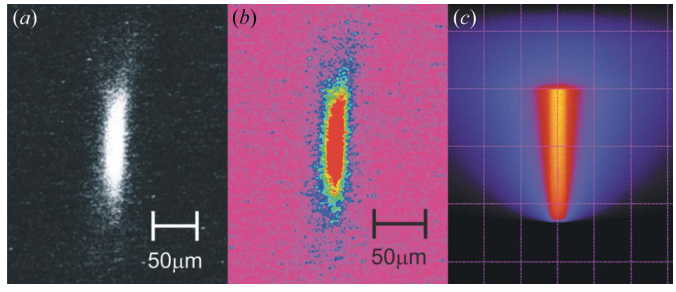

Figure 8
Comparison of detected focal spot (*a*) with the intensity profile of the detected focal spot (*b*) and the simulated focal spot (*c*).

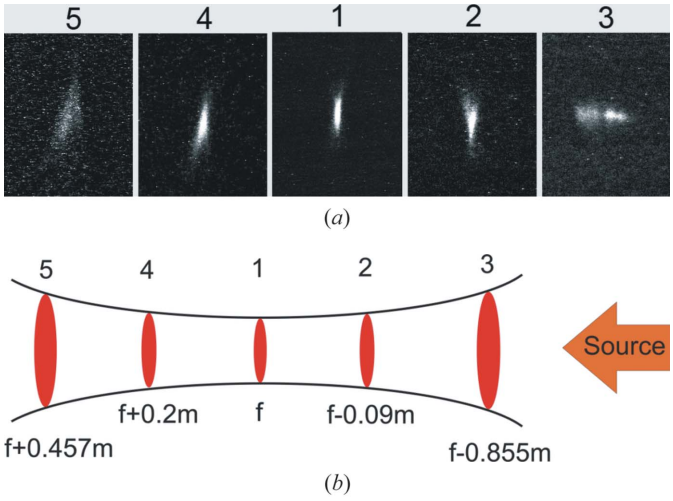

Figure 9
(*a*) Different focal spot sizes at different focal distances. (*b*) Schematic behaviour of the focal spot size at different distances from the focusing distance.

calculated focus distance was 1.1 m, making a ratio of 31.728. If the source size was 270 µm then the expected focal spot should be just 8.5 µm, which is only one pixel. Taking into account crystal misalignment, a measured focus distance of 1.405 m and the detector spread function, a focal spot of 10.86 µm should be detected. Instead we measured a 3.5 times larger focal spot. Reasons for this mismatch are the imperfect mutual alignment of the two crystals and the tilt with respect to the vertical scattering plane.

The second crystal had all possible freedoms of movement, so its alignment was very easy, but the first crystal was mounted on a goniometer head which had no possibility of this tilt movement, so the crystal was slightly unparallel with the second crystal. Nevertheless, the focal spot shape of the low-aberration simulation is identical to the detected focal spot. In Figs. 9(*a*) and 9(*b*) we present an evolution of the focal spot size at different distances around the focal distance. If one sets the focal distance as zero, slide 1, then slides 2 and 3 represent the focal spot size at 0.09 m and 0.855 m from the focal distance (towards the source). Slides 4 and 5 represents the focal spot size at 0.2 m and 0.457 m from the focal distance in the other direction (from the source). Fig. 9(*b*) shows the schematic behaviour of the focal spot shape.

Even if we have mechanochemically polished the internal walls of the crystals the achieved surface quality was not as high as for flat Si surfaces and there were visible marks from the drilling tool. This leads to a broadening of the focal spot for the surface-sensitive grazing-incidence geometry which we have used.

5. Conclusions

Two asymmetrically cut Si(111) Bragg crystals with a precise parabolic groove were aligned to demonstrate experimentally a low-aberration focus for the first time. The detected focal spot had the same shape as the ray-tracing simulation. The disagreement between the calculated focal distance, 1.1 m, and measured focal distance, 1.405 m, and the different focal spot sizes, 38.25 µm *versus* 10.86 µm, was attributed to the misalignment of the two crystals and small imperfections of the surface quality. Further improvement can be made by achieving a better surface quality with non-contact polishing methods such as ion beam figuring (Wilson *et al.*, 1988; Ziegler *et al.*, 2009). The measured focal spot size was by far the smallest one achieved with this kind of crystal optical device. Smaller focusing distances could be achieved if one uses a stock of crystals aligned in a series, because the focusing distance is inversely proportional to the number of diffraction events (crystal surfaces). Another improvement could be made by choosing a different asymmetry angle; this way one can enlarge the already large acceptance of the focusing device.

This research was supported by the Grant Agency of the Academy of Sciences of the Czech Republic, No. IAA 100100716, and the Institutional Research Plan of ASCR, No. AVOZ 10100522, the Ministry of Education of the Czech Republic (MSM 0021622410) and FR-TI1/412. The Si crystals were produced by Polovodiče a.s. We would like to thank the crystal workshop of the Physics Institute of the Academy of Sciences of the Czech Republic for preparing the crystals.

References

Artemiev, N., Hrdý, J., Bigault, T. & Peredkov, S. (2003). *Proc. SPIE*, **5195**, 104–108.
Beaumont, J. H. & Hart, M. (1974). *J. Phys. E*, **7**, 823–829.
Hrdá, J., Hrdý, J., Hignette, O. & Hoszowska, J. (2003). *Proc. SPIE*, **5195**, 109–114.
Hrdá, J., Potlovskiy, K. & Šlechtová, V. (2005). *J. Phys. D*, **38**, A223–A226.
Hrdý, J. (1998). *J. Synchrotron Rad.* **5**, 1206–1210.
Hrdý, J., Artemiev, N., Freund, A. & Quintana, J. P. (2001). *Proc. SPIE*, **4501**, 88–98.
Hrdý, J., Kuběna, A. & Mikulík, P. (2005). *J. Phys. D*, **38**, 4325–4328.
Hrdý, J., Mocella, V., Oberta, P., Peverini, L. & Potlovskiy, K. (2006). *J. Synchrotron Rad.* **13**, 392–396.
Hrdý, J. & Oberta, P. (2008). *Rev. Sci. Instrum.* **79**, 073105.
Hrdý, J. & Siddons, D. P. (1999). *J. Synchrotron Rad.* **6**, 973–978.
Korytár, D., Mikulík, P., Ferrari, C., Hrdý, J., Baumbach, T., Freund, A. & Kuběna, A. (2003). *J. Phys. D*, **36**, A65–A68.
Krisch, M., Freund, A., Marot, G. & Zhang, L. (1990). *Nucl. Instrum. Methods Phys. Res. A*, **305**, 208–213.
Sparks, C. J., Ice, G. E., Wong, J. & Batterman, B. W. (1982). *Nucl. Instrum. Methods*, **195**, 73–78.
Wilson, S. R., Reicher, D. W. & McNeil, J. R. (1988). *Proc. SPIE*, **966**, 74–81.
Ziegler, E., Peverini, L., Kozhevnikov, I., Rommeveaux, A., Vaxelaire, N., Claustre, L., Van Vaerenbergh, P., Guillet, S., Massonnat, J. & Susini, J. (2009). *Proceedings of the 10th International Conference on Synchrotron Radiation Instrumentation (SRI'09)*, Melbourne, Australia, 27 September–2 October 2009.